Politecnico di Torino

Porto Institutional Repository

[Article] Energy transfer and energy level decay processes in Tm3+-doped tellurite glass

(Article begins on next page)

Laércio Gomes, Joris Lousteau, Daniel Milanese, Gerardo C. Scarpignato, and Stuart D. Jackson

Related Articles

Additional information on J. Appl. Phys.

Energy transfer and energy level decay processes in Tm³⁺-doped tellurite glass

Laércio Gomes,[1] Joris Lousteau,[2] Daniel Milanese,[2] Gerardo C. Scarpignato,[2] and Stuart D. Jackson[3,a)]

[1]*Instituto de Pesquisas Energéticas e Nucleares, Centro de Lasers e Aplicações, P.O. Box 11049, São Paulo, SP 05422-970, Brazil*
[2]*PhotonLab, Dipartimento di Scienza dei Materiali ed Ingegneria Chimica, Politecnico di Torino, C.so Duca degli Abruzzi 24, 10129 Torino, Italy*
[3]*Institute of Photonics and Optical Science, School of Physics, University of Sydney, Camperdown, 2006, Australia*

The primary excited state decay and energy transfer processes in singly Tm³⁺-doped TeO₂:ZnO:Bi₂O₃:GeO₂ (TZBG) glass relating to the $^3F_4 \rightarrow \, ^3H_6$ ~1.85 μm laser transition have been investigated in detail using time-resolved fluorescence spectroscopy. Selective laser excitation of the $^3H_4$ manifold at 794 nm, the $^3H_5$ manifold at 1220 nm, and $^3F_4$ manifold at 1760 nm has established that the $^3H_5$ manifold is entirely quenched by multiphonon relaxation in tellurite glass. The luminescence from the $^3H_4$ manifold with an emission peak at 1465 nm suffers strong suppression due to cross relaxation that populates the $^3F_4$ level with a near quadratic dependence on the Tm³⁺ concentration. The $^3F_4$ lifetime becomes longer as the Tm³⁺ concentration increases due to energy migration and decreases to 2.92 ms when [Tm³⁺] = 4 mol. % as a result of quasi-resonant energy transfer to free OH⁻ radicals present in the glass at concentrations between 1×10^{18} cm⁻³ and 2×10^{18} cm⁻³. Judd-Ofelt theory in conjunction with absorption measurements were used to obtain the radiative lifetimes and branching ratios of the energy levels located below 25 000 cm⁻¹. The spectroscopic parameters, the cross relaxation and Tm³⁺($^3F_4$) → OH⁻ energy transfer rates were used in a numerical model for laser transitions emitting at 2335 nm and 1865 nm. © *2012 American Institute of Physics*. [http://dx.doi.org/10.1063/1.3694747]

I. INTRODUCTION

There is strong interest in the development of fiber laser systems capable of delivering efficient high power output at a wavelength of 2 μm and beyond. To date, the most successful shortwave infrared fiber laser involves silicate glass fibers and the Tm³⁺ ion[1] and many variants of this fiber laser have now been demonstrated. Recently,[2] an efficient Tm³⁺-doped tellurite glass fiber laser operating on the $^3F_4 \rightarrow \, ^3H_6$ laser transition was demonstrated that produced a record slope efficiency of 76%. In a double-clad arrangement, Tm³⁺-doped tellurite glass fiber lasers have been shown to be capable of approximately 1 W output.[3] These encouraging results extend previous work on tellurite glasses designed for upconversion emission,[4] Tm³⁺, Ho³⁺ co-doping,[5] Tm³⁺, Er³⁺ co-doping,[6] emission at 1.2 μm,[7] and emission at 1.47 μm.[8] These studies highlight the broad capabilities of tellurite glasses and compliment previous successful studies relating to other heavy metal oxide glasses, for example, the germanates.[9]

The use of tellurite glass in laser research introduces a number of important characteristics to the field including comparatively large rare earth ion solubility, a smaller maximum phonon energy compared to the other oxide glasses used for shortwave emission, and a comparatively large refractive index that creates large absorption and emission cross sections. These features make Tm³⁺-doped tellurite glass fibers particularly suitable for short length fiber lasers that deliver a narrow linewidth or pulses at a high repetition rate.

To augment the experimental demonstrations of Tm³⁺-doped tellurite fiber lasers, a detailed spectroscopic analysis that can facilitate numerical modeling and hence future optimization is required. There have been a small number of spectroscopic analyses of Tm³⁺-doped tellurite glass,[10–12] however, a more detailed investigation examining the various energy transfer processes, as a function of Tm³⁺ concentration is necessary. In addition, the requirement for fiber lasers to emit longer wavelengths grows thus necessitating a spectroscopic investigation and numerical modeling study of the emission at 2.3 μm that arises from the $^3H_4 \rightarrow \, ^3H_5$ transition of Tm³⁺. In a similar way to the $^3F_4 \rightarrow \, ^3H_6$ laser transition, the efficiency of this transition is highly concentration dependent and the rate parameters for cross relaxation must be determined so that optimal fiber arrangements are found.

In this investigation we present a time resolved spectroscopic study of Tm³⁺-doped tellurite glass based on a recently developed TeO₂:ZnO:Bi₂O₃:GeO₂ (TZBG) glass. We have prepared a number of Tm³⁺-doped TZBG samples of varying Tm³⁺ concentration and measured the luminescence decay characteristics after selective energy level excitation. The luminescence efficiencies of these levels were determined when the experimental decay time was compared

a)Author to whom correspondence should be addressed. Electronic mail: s.jackson@usyd.edu.au.

with the radiative lifetimes calculated using Judd-Ofelt theory. The results from the spectroscopic measurements we then used as parameters for a numerical model, which was used to understand the performance of Tm^{3+}-doped tellurite fiber lasers operating on shortwave infrared transitions.

II. EXPERIMENTAL PROCEDURE

The Tm^{3+}-doped tellurite (TZBG) glass samples used for the time-resolved luminescence spectroscopy measurements were prepared from the raw materials: 99+% TeO_2; 99.99%, ZnF_2, and Bi_2O_3; and 99.999% GeO_2. The glass composition was $(100-x)$ [76 TeO_2 – 12.5 ZnF_2 – 5 Bi_2O_3 – 6.5 GeO_2] – x [Tm_2O_3] with $x = 0.25$, 0.5, 1, and 2 mol %. The starting powder materials were melted in a Pt crucible in a dry glovebox environment at 900 °C to reduce iOH^- content in the glass. The molten liquids were poured into polished brass molds and annealed at around T_g to remove any mechanical stress. The glass host density was 5.86 g cm^{-3} and the measured refractive index was 2.06 at 1533 nm. The samples were cut and polished into $4.6 \times 10 \times 15$ mm rectangular prisms. The Tm^{3+} ion density was calculated to be 1.07×10^{20} cm^{-3}, 2.14×10^{20} cm^{-3}, 4.27×10^{20} cm^{-3}, and 8.46×10^{20} cm^{-3} for the tellurite samples having Tm^{3+} ion concentrations of 0.5, 1, 2, and 4 mol. %, respectively.

The optical absorption spectrum of the Tm^{3+} ions doped into tellurite glass has three main features in the near to shortwave infrared, one feature is located at approximately 1767 nm and arises from the $^3H_6 \rightarrow {}^3F_4$ transition, a second feature is located at approximately 1230 nm arises from the $^3H_6 \rightarrow {}^3H_5$ transition, and a third feature located at approximately 800 nm arises from the $^3H_6 \rightarrow {}^3H_4$ transition. When Tm^{3+}-doped tellurite glass is excited with light in the range 792-805 nm the following processes are known to occur:

(a) Ground state absorption (GSA): Tm^{3+} ($^3H_6$) + hν (800 nm) $\rightarrow Tm^{3+}$ ($^3H_4$);

(b) Cross-relaxation (CR): Tm^{3+} ($^3H_4$) + Tm^{3+} ($^3H_6$) $\rightarrow$ Tm^{3+} ($^3F_4$) + Tm^{3+} ($^3F_4$).

The CR process is perhaps the most important energy transfer process in shortwave infrared fiber laser research because it allows a single pump photon to create, at least theoretically, two excited Tm^{3+} ions.[13] After the excitation of Tm^{3+}, the $^3F_4 \rightarrow {}^3H_6$ laser transition at approximately 1.9 μm can operate with at high slope efficiency when the concentration of Tm^{3+} ions is sufficiently high. In contrast, CR can reduce the efficiency of the $^3H_4 \rightarrow {}^3H_5$ transition, which requires a considerable population to reside in the $^3H_4$ level. Thus the Tm^{3+} concentrations specific to each transition requires a detailed understanding of the rate of CR as a function of [Tm^{3+}].

The absorption spectra in the range between 2000 and 10 000 nm were measured using a FTIR spectrophotometer (Nicolet 6700). The decay characteristics of the excited states of Tm^{3+} were measured using pulsed 9 mJ 4 ns laser excitation from a tunable optical parametric oscillator (OPO) pumped by the second harmonic of a Q-switched Nd-YAG laser (Brilliant B from Quantel). Tunable laser excitation from the OPO was used to directly excite the $^3H_4$ and $^3F_4$ energy levels at 795 nm and 1600 nm, respectively. The

luminescence was detected using an InSb infrared detector (Judson model J-10 D cooled to 77 K) in conjunction with a fast preamplifier with a response time of $\sim 0.5 \mu$s and analyzed using a digital 200 MHz oscilloscope (Tektronix TDS 410). All the fluorescence decay characteristics were measured at 300 K. To isolate the luminescence signals, bandpass filters each with $\sim 80\%$ transmission at 1450 nm or 1850 nm with a half width of 25 nm and an extinction coefficient of $\sim 10^{-5}$ outside this band were used. The infrared emission spectrum was measured from 1200 nm to 3000 nm using a Boxcar technique working in the static gate mode (gate = 1 μs) and a 0.25 m monochromator with a spectral grating blazed for 2100 nm and an InSb (77 K) infrared detector and a silicon filter at the monochromator entrance.

III. EXPERIMENTAL RESULTS

Figure 1 shows the visible to shortwave infrared (a) and midwave infrared (b) absorption spectra of Tm^{3+} (1 mol %)-doped tellurite glass. The spectrum shows a broad strong absorption band between 2500 and 3500 cm^{-1}, which we attribute to free OH^- groups.[14] The concentration of OH^- radicals is given by $N_{OH} = N_A \alpha / N_A \alpha \xi$, where N_A is Avogadro's constant (6.02×10^{23}), α is the absorption coefficient (= 0.1574 cm^{-1} for 1 mol % Tm^{3+}) relevant to the OH^-
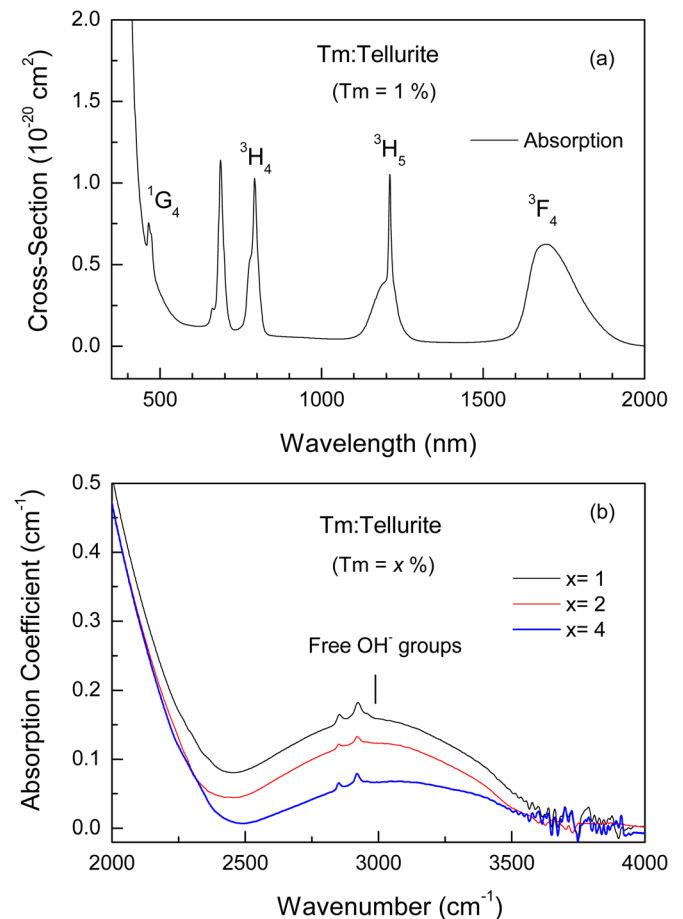

FIG. 1. Measured absorption spectra in the (a) visible and shortwave infrared region and (b) OH^- vibration feature in Tm^{3+} (0.5, 1, 2, and 4 mol %)-doped TZBG glasses (sample thickness 4.6 mm). $\sigma_{abs} = 1.02 \times 10^{-20}$ cm^2 for the $^3H_6 \rightarrow {}^3H_4$ transition at 794 nm.

TABLE I. Comparison of J-O parameters with the literature.[a]

Reference	Ω_2	Ω_4	Ω_6
17[b]	3.38	2.17	1.17
18[b]	4.64	1.61	1.26
19[c]	5.106	1.174	1.082
20[b]	4.4	1.97	1.22
This study[d]	3.23	1.26	0.83

[a]$\Omega[10^{-20}$ cm$^2]$.
[b]Host composition: 75TeO$_2$-20ZnO-5Na$_2$O.
[c]Host composition: 80TeO$_2$-10ZnO-10Na$_2$O.
[d]Host composition: 76TeO$_2$-12.5ZnF$_2$-5Bi$_2$O$_3$-6.5GeO$_2$.

vibration band at 3000 cm^{-1}, and ξ is the absorptivity of free OH$^-$ groups in the glass. Using $\xi = 49.1 \times 10^3$ cm^2 mol^{-1},[15] we estimated the OH$^-$ concentration in our samples to be 2×10^{18} cm^{-3} (for 0.5 mol % Tm^{3+}), 1.9×10^{18} cm^{-3} (for 1 mol % Tm^{3+}), 1.5×10^{18} cm^{-3} (for 2 mol % Tm^{3+}), and 0.97×10^{18} cm^{-3} (for 4 mol % Tm^{3+}). These values are approximately 76 times smaller than the free OH$^-$ density (2.4×10^{19} cm^{-3}) found in Er^{3+}-doped germanotellurite glass produced from drying the melt using oxygen gas and CCl$_4$ bubbling.[16]

A. Calculation of the radiative lifetimes

The absorption transitions originating from the ground state are spectroscopically assigned as $^1G_4$, $^3F_{2,3}$, $^3H_4$, $^3H_5$ and $^3F_4$ (see Fig. 1). Judd-Ofelt theory was used to calculate the transition probabilities between the different manifolds, the radiative lifetimes, and the branching ratios as found in the literature.[17,18] The Judd-Ofelt parameters were determined using the five main absorption bands and are summarized in Table I together with the literature overview. The absorption bands of Tm^{3+} are dominated by electric dipole transitions except the $^3H_6 \rightarrow {}^3H_5$ transition, which contains contributions from electric-dipole and magnetic-dipole transitions and which can be easily calculated.[18] The largest error in the Judd-Ofelt calculation relates to the assumption

that all Stark levels of a given multiplet are equally populated. A summary of the radiative rates, lifetimes and branching ratios of the main transitions is given in Table II.

B. Infrared fluorescence spectrum of Tm^{3+} in tellurite (TZBG) glass

The fluorescence emission spectrum of Tm^{3+} in the shortwave infrared was measured for [Tm^{3+}] = 4 mol %. Figure 2 shows that there are three emission bands; two initiating from the $^3H_4$ level at ~1465 nm and ~2320 nm and one initiating from the $^3F_4$ level at ~1850 nm. The strong emission band at ~1850 nm is boosted by CR that decreases the luminescence efficiency of the $^3H_4$ level and consequently increases emission from the $^3F_4$ level. As a consequence, the emission band near 2320 nm (from the $^3H_4$ level) decreases. The emission cross-section of the $^3H_4 \rightarrow {}^3H_5$ and $^3F_4 \rightarrow {}^3H_6$ transitions was calculated using

$$\sigma_{emis}(\lambda) = \frac{(\bar{\lambda})^4}{8\pi n^2 c} A_{JJ'}\varepsilon(\lambda), \tag{1}$$

where $\varepsilon(\lambda) = S(\lambda)/\int S(\lambda)d\lambda$ is the line-shape of the emission band, c is the speed of light, and n is the refractive index (n = 2). Using $\bar{\lambda} = 1854$ nm (centroid), $A_{JJ'} = 369$ s^{-1} and $\varepsilon(\lambda) = 4.22 \times 10^{-3}$ nm^{-1} we have $\sigma_{emis} = 6.11 \times 10^{-21}$ cm^2 for the $^3F_4 \rightarrow {}^3H_6$ transition near 1854 nm. Using $\bar{\lambda} = 2336$ nm (centroid), $A_{JJ'} = 62$ s^{-1} and $\varepsilon(\lambda) = 5.11 \times 10^{-3}$ nm^{-1} one has $\sigma_{emis} = 3.13 \times 10^{-21}$ cm^2 for the $^3H_4 \rightarrow {}^3H_5$ transition.

The emission cross-section values obtained for emission from the $^3H_4$ and $^3F_4$ levels are 5.1×10^{-21} cm^2 at 1465 nm, 3.1×10^{-21} cm^2 at 2336 nm, and 6.1×10^{-21} cm^2 at 1854 nm, respectively for Tm-doped tellurite (TZBG) glass. These values are in agreement with those reported in the literature for other tellurite glasses[18,19,21] and higher than those reported in fluoride and oxyfluoride glasses.[22]

C. Emission decay from the $^3H_4$ level

Figure 3 shows the emission decay characteristic at 1500 nm (from the $^3H_4 \rightarrow {}^3F_4$ transition) for [Tm^{3+}] = 0.5, 1,

TABLE II. Transition rates, radiative lifetimes (τ_R), and branching ratios (β).

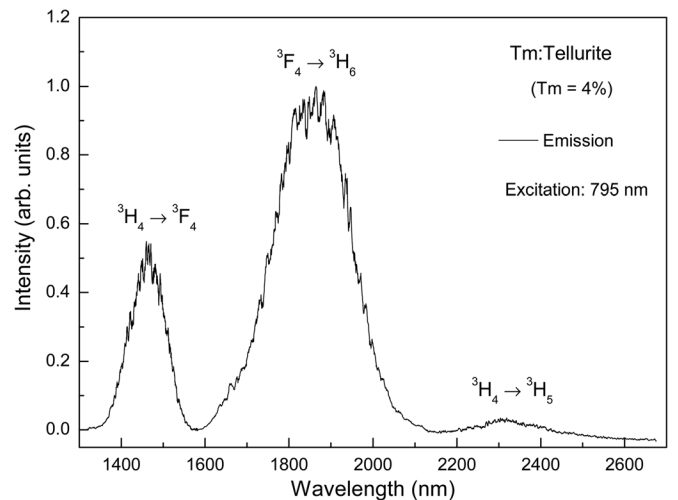| Transition	$\bar{\lambda}$ (nm)	$A_{JJ'}$ (s^{-1})	τ_R (ms)	β
$^1G_4 \rightarrow {}^3H_6$	473	2259.8	0.241	0.5445
$^1G_4 \rightarrow {}^3F_4$	645	293.8		0.0708
$^1G_4 \rightarrow {}^3H_5$	768	1125.9		0.2713
$^1G_4 \rightarrow {}^3H_4$	1157	369.3		0.0890
$^1G_4 \rightarrow {}^3F_3$	1472	79.8		0.0192
$^3F_3 \rightarrow {}^3H_6$	696	3248.8	0.247	0.8034
$^3F_3 \rightarrow {}^3F_4$	1149	243.2		0.0601
$^3F_3 \rightarrow {}^3H_5$	1607	546.2		0.1351
$^3F_3 \rightarrow {}^3H_4$	5411	5.4		0.0013
$^3H_4 \rightarrow {}^3H_6$	799	2060.7	0.435	0.8973
$^3H_4 \rightarrow {}^3F_4$	1459	173.7		0.0756
$^3H_4 \rightarrow {}^3H_5$	2286	62.0		0.0270
$^3H_5 \rightarrow {}^3H_6$	1229	498.9	1.96	0.9789
$^3H_5 \rightarrow {}^3F_4$	4035	10.7		0.0211
$^3F_4 \rightarrow {}^3H_6$	1767	368.9	2.71	1

FIG. 2. Emission spectrum of Tm^{3+}(4 mol %)-doped TZBG glass using pulsed laser excitation at 795 nm with 9 mJ pulses of 4 ns duration and 10 Hz repetition rate.
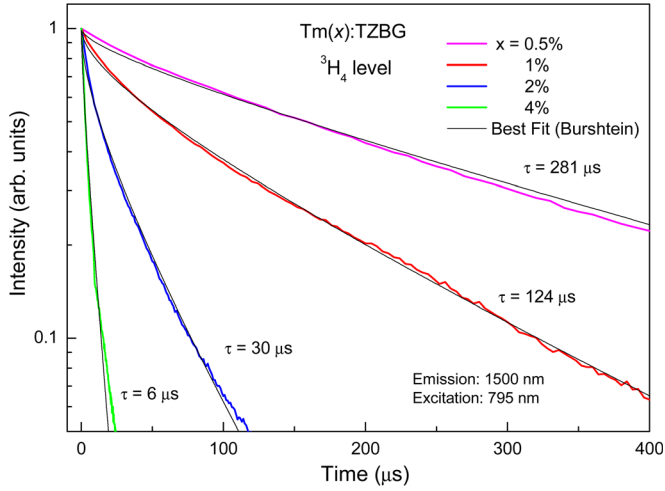
FIG. 3. Measured decay time of the $^3H_4$ level (emission at 1500 nm) after laser excitation at 795 nm, 9 mJ pulses of 4 ns duration (colored solid lines) for the $Tm^{3+}(x)$-doped samples with $x = 0.5$, 1, 2, and 4 mol %. The best fit to the decay time using Eq. (2) provided having R^2 values of 0.998 for $[Tm^{3+}] = 0.5\%$, 0.992 for $[Tm^{3+}] = 1\%$, 0.995 for $[Tm^{3+}] = 2\%$, and 0.984 for $[Tm^{3+}] = 4\%$.

2, and 4 mol % after laser excitation at 795 nm with a mean pulse energy of 9 mJ and 4 ns duration. The luminescence decay of the $^3H_4$ excited state was nonexponential and was fitted using the Burshtein model,[23] obtaining

$$I(t) = I_0 \exp(-\gamma \sqrt{t} - t/\tau_m), \quad (2)$$

where $\gamma(s^{-1/2})$ is the transfer constant due to the direct donor to acceptor transfer and τ_m is defined by

$$1/\tau_m = 1/\tau_R + W_{nR} + \omega, \quad (3)$$

where τ_R is the radiative lifetime and ω is the transfer constant (s^{-1}) due to the migration assisted donor to acceptor transfer. W_{nR} is the nonradiative multiphonon decay rate (s^{-1}), which is neglected for the $^3H_4$ level (because $W_{nR} \sim 0$). The luminescence decay of the $^3H_4$ level at 1500 nm was nonexponential and the effective $^3H_4$ lifetime (τ) was obtained by integration[24] using

$$\tau = \frac{1}{I_0} \int_0^\infty I(t) dt. \quad (4)$$

The best fit to the measured 1500 nm luminescence decay curve was carried out using Eq. (3); see solid line in Fig. 3 where the fitting parameters are: (*i*) $\gamma = 24.9 \, s^{-1/2}$ and $\tau_m = 417.1 \, \mu s$ ($\omega = 98.5 \, s^{-1}$), for $[Tm^{3+}] = 0.5\%$; (*ii*) $\gamma = 58.2 \, s^{-1/2}$ and $\tau_m = 254.9 \, \mu s$ ($\omega = 1624 \, s^{-1}$), for $[Tm^{3+}] = 1\%$; (*iii*) $\gamma = 146 \, s^{-1/2}$ and $\tau_m = 75.8 \, \mu s$ ($\omega = 10\,894 \, s^{-1}$), for $[Tm^{3+}] = 2\%$, and (*iv*) $\gamma = 214 \, s^{-1/2}$ and $\tau_m = 9.3 \, \mu s$ ($\omega = 105\,649 \, s^{-1}$), for $[Tm^{3+}] = 4\%$.

The effective lifetime (τ) of the $^3H_4$ level was obtained by integration using Eq. (4) given the following values: $\tau = 281 \, \mu s$ for $[Tm^{3+}] = 0.5 \, mol \, \%$, $124 \, \mu s$ (for $[Tm^{3+}] = 1\%$), $30 \, \mu s$ (for $[Tm^{3+}] = 2\%$), and $6 \, \mu s$ (for $[Tm^{3+}] = 4\%$). The following luminescence efficiencies (η_1) were derived from the lifetime measurements: (*i*) 58% for
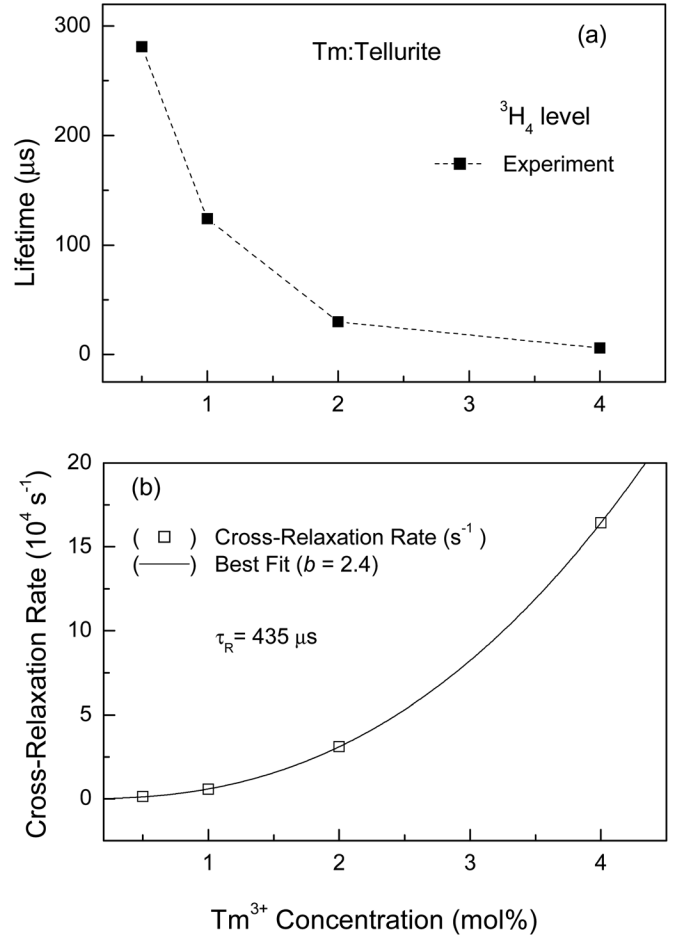

FIG. 4. (a) Measured lifetime of the $^3H_4$ level (1500 nm) for the $Tm(x)$-doped TZBG glass, where $x = 0.5$, 1, 2, and 4 mol % and (b) the cross-relaxation rate (s^{-1}) as a function of $[Tm^{3+}]$. Solid line in (b) represents the best fit using a power law, $W_{CR} = a \, x^{b}$, where the fitting parameters are $a = 5854.4 \, (mol \, \%)^{-1} \, s^{-1}$ and $b = 2.4$.

$[Tm^{3+}] = 0.5\%$; 25.6% for $[Tm^{3+}] = 1\%$; 6.2% for $[Tm^{3+}] = 2\%$ and 1.2% for $[Tm^{3+}] = 4\%$ for 800 nm emission ($^3H_4 \rightarrow \,^3H_6$); (*ii*) 4.9% for $[Tm^{3+}] = 0.5\%$; 2.2% for $[Tm^{3+}] = 1\%$; 0.52% for $[Tm^{3+}] = 2\%$; 0.1% for $[Tm^{3+}] = 4\%$ for 1865 nm emission ($^3H_4 \rightarrow \,^3F_4$); and (*iii*) 1.74% for $[Tm^{3+}] = 0.5\%$; 0.77% for $[Tm^{3+}] = 1\%$; 0.19% for $[Tm^{3+}] = 2\%$; 0.037% for $[Tm^{3+}] = 4\%$ for 2335 nm emission ($^3H_4 \rightarrow \,^3H_5$).

The decrease in the effective lifetime of the $^3H_4$ level is due to the rate of CR (process *b*), which competes with the intrinsic level decay. The cross-relaxation rate (s^{-1}) was obtained using the following relation:

$$W_{CR} = \frac{1}{\tau} - \frac{1}{\tau_R}. \quad (5)$$

Using $\tau_R = 435 \, \mu s$ and the above values of τ (= τ_4) we get $W_{CR} = 1262 \, s^{-1}$ for $[Tm^{3+}] = 0.5\%$, $5768 \, s^{-1}$ (for $[Tm^{3+}] = 1\%$), $31\,068 \, s^{-1}$ (for $[Tm^{3+}] = 2\%$) and $164\,369 \, s^{-1}$ (for $[Tm^{3+}] = 4\%$). Figure 4(a) shows the measured lifetime of the $^3H_4$ level for Tm^{3+}-doped TZBG glasses as a function of $[Tm^{3+}]$ (in mol%). Figure 4(b) shows the cross-relaxation rate (s^{-1}) as a function of the $[Tm^{3+}]$, where it is observed that W_{CR} is proportional to $[Tm^{3+}]^{b=2.4}$. A value of $b \sim 2$ is expected, however, for a diffusion limited CR process.[25]

D. Emission decay from the $^3F_4$ level

Figure 5 shows the emission decay from the $^3F_4$ level measured at 1850 nm after pulsed laser excitation at 1600 nm (E = 9 mJ). The emission decay from the $^3F_4$ state is observed to be quasi-exponential because the $\gamma(exp)$ values are quite small ($\gamma \sim 3$ s$^{-1/2}$), which indicates the presence of weak energy transfer to free OH$^-$ radicals. The luminescence decay of the $^3F_4$ excited state, however, was fitted using the Burshtein model [Eq. (2)]; see the black solid line in Fig. 5. The fitting parameters were: (*i*) $\gamma = 5.1$ s$^{-1/2}$ and $\tau_m = 5.25$ ms for [Tm^{3+}] = 0.5%; (*ii*) $\gamma = 3.5$ s$^{-1/2}$ and $\tau_m = 5.25$ ms for [Tm^{3+}] = 1%; (*iii*) $\gamma = 3.1$ s$^{-1/2}$ and $\tau_m = 4.82$ ms for [Tm^{3+}] = 2%; and (*iv*) $\gamma = 3$ s$^{-1/2}$ and $\tau_m = 3.16$ ms for [Tm^{3+}] = 4 mol%. W_{nR}, the nonradiative multiphonon decay rate (s^{-1}), is neglected for the $^3F_4$ level, i.e., $W_{nR} \sim 0$.

The effective lifetime (τ) of the $^3F_4$ level was obtained using Eq. (4). It can be observed from Fig. 6 that the $^3F_4$ decay time initially increases with the increasing Tm^{3+} concentration up to [Tm^{3+}] ≈ 2 mol % and the values display a slight decrease to [Tm^{3+}] = 4 mol %. The measured decay

times for the $^3F_4$ level are longer than the calculated radiative lifetime ($\tau_R = 2.71$ ms, calculated above using Judd-Ofelt theory). The increased value of the decay time of the $^3F_4$ level in our experiment relates to strong excitation migration from nonradiative resonant dipole-dipole interaction between the $^3F_4$ and the $^3H_6$ energy levels. This phenomenon explains the initial increase in the decay time as the Tm^{3+} concentration is increased. Note that measuring the luminescence close to the pumped surface can minimize radiation trapping. In our experiment, we observed an increase in the decay time at distances perpendicular to the pump of ~ 8 mm, however, for distances of ~ 3 mm and shorter (from where we took the measurements) the measured decay time was invariable.

The line of best fit to the decay time characteristic (open circles in Fig. 6) with the increase in [Tm^{3+}] was carried out using Eq. (6) which predicted that the lifetime of the $^3F_4$ level increases if a Tm^{3+} ion that is excited to the $^3F_4$ level transfers excitation to a ground state Tm^{3+} ion within a critical distance, R_C, with a decay time augmentation efficiency, η, dependent on the Tm^{3+} concentration.[26] This model predicts a saturation of the decay time increase to a value ($\tau_R + \tau_0$), which should be reached for $N_{Tm} > N_C$, where N_C is the critical concentration which can be calculated from

$$\eta(Tm) = 1 - \exp(-N_{Tm}/N_C); \quad \tau_d = \tau_R + \eta(Tm)\tau_0. \quad (6)$$

The best fit using Eq. (6) gives $\tau_0 = 1.77$ ms, $N_C = 0.345$ mol % and $\tau_R = 2.65$ ms (R$^2 = 0.976$), see solid line in Fig. 6.

No up-conversion processes, i.e., excited state absorption (ESA) or energy transfer upconversion (ETU) initiating from the $^3F_4$ or $^3H_4$ levels was observed in our measurements using pulsed 4 ns laser excitation at 795 nm or 1600 nm with a mean energy of ~ 9 mJ for the samples having [Tm^{3+}] ≤ 4 mol %.
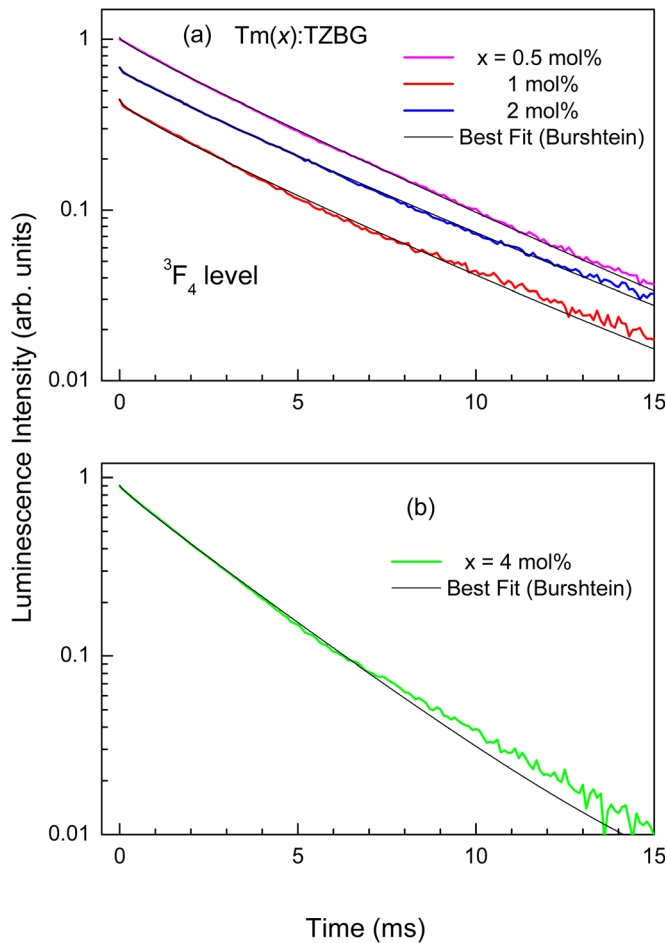

FIG. 5. Measured emission decay of the $^3F_4$ excited state at 1850 nm for (a) [Tm^{3+}] = 0.5, 1, 2 mol % and (b) [Tm^{3+}] = 4 mol % after laser excitation at 1600 nm with a mean energy of ~ 9 mJ and 4 ns pulse duration. The best fit to the decay time using Eq. (2) provided R^2 values of 0.9991 for [Tm^{3+}] = 0.5%, 0.9997 for [Tm^{3+}] = 1%, 0.995 for [Tm^{3+}] = 2%, and 0.9995 for [Tm^{3+}] = 4%.
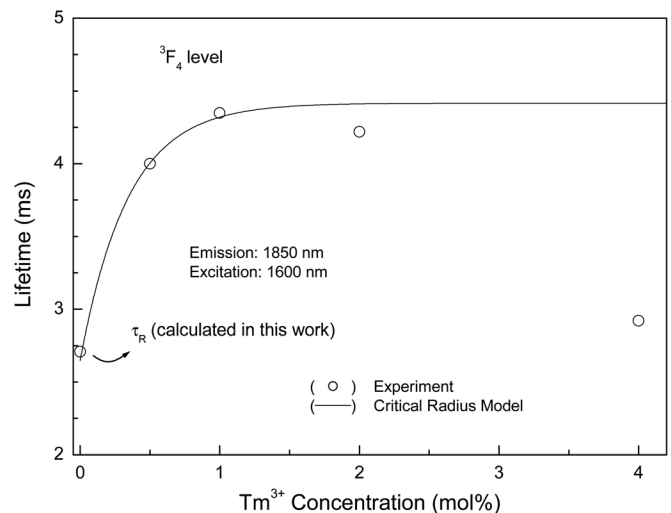

FIG. 6. Measured decay time (τ) of $^3F_4$ level measured at 1850 nm using laser excitation at 1600 nm (E = 9 mJ, 4 ns) for Tm^{3+}-doped TZBG glass as a function of [Tm^{3+}]. The solid line represents the best fit using the critical radius model given by Eq. (6), where $\tau_R = 2.71$ ms, and the fitting parameters were $\tau_0 = 1.77$ ms and $N_C = 0.345$ mol % (R$^2 = 0.976$).

IV. DISCUSSION

The excitation pulse used to investigate the luminescence properties had a mean pulse energy of $\sim$10 mJ, 4 ns pulse duration and a beam area of $\sim$4.5 mm^2 providing an average intensity of $\sim$56 MW cm^{-2} on the sample. This pump intensity could easily create energy ETU and two-photon absorption (TPA) processes, which can produce observable visible or near infrared luminescence. Upconversion luminescence, however, was not observed in the Tm-doped tellurite (TZBG) glass used in this work after the excitation wavelengths were scanned in the following spectral ranges: (*i*) from 1500 nm to 2000 nm ($^3H_6 \rightarrow {}^3F_4$) to create upconversion luminescence at 1465 nm from the $^3H_4$ level; (*ii*) from 1100 nm to 1450 nm ($^3H_6 \rightarrow {}^3H_5$) to create upconversion luminescence at 2335 nm from the $^3H_4$ level; (*iii*) from 700 nm to 900 nm ($^3H_6 \rightarrow {}^3F_4$) to create upconversion luminescence (at 470 nm to 490 nm) from the $^1G_4$ level. Our conclusion is that TPA is not possible from the three lowest excited states of Tm^{3+} in tellurite (TZBG) glass and ETU was not observed from the $^3F_4$ excited level at least for [Tm^{3+}] = 4%. The high refractive index of tellurite glass (n = 2) suggests the possible creation of nonlinear effects such as second harmonic generation, thermal lensing or color center formation, however the effects from these processes were not observed for pulsed excitation at 794 nm, 1220 nm or 1760 nm at a excitation mean intensity of $\sim$56 MW cm^{-2}.

The reduction of the $^3F_4$ decay time observed for the case of [Tm] = 4 mol % (see data in Fig. 6) may indicate energy transfer from the $^3F_4$ level to the OH$^-$ radical whose relevant absorption band is shown in Fig. 1(b) for Tm^{3+}-doped TZBG glass. A partial overlap between the $^3F_4 \rightarrow {}^3H_6$ emission band of Tm^{3+} (with a maximum at $\sim$5360 cm^{-1}) and the free OH$^-$ radical absorption ($\nu = 0 \rightarrow \nu = 2$) (with absorption between 5000 and 7000 cm^{-1}) clearly exists and the energy transfer should be dominated by excitation migration of the $^3F_4$ level. The energy transfer process Tm$^{3+} \rightarrow$ OH$^-$ was investigated using the data in Fig. 6 by taking the difference between the calculated lifetime (τ_d) that contains the migration effects and the effective lifetime (τ). The rate of energy transfer W_{OH} is given by

$$W_{OH} = \frac{1}{\tau_d} - \frac{1}{\tau}. \tag{7}$$

The following W_{OH} transfer rates were obtained for the Tm^{3+}-doped TZBG glasses: (*i*) $W_{OH} \sim 0$ for [Tm^{3+}] = 0.5 and 1 mol %, (*ii*) $W_{OH} \sim 10$ s^{-1} for [Tm] = 2 mol %, and (*iii*) $W_{OH} = 116$ s^{-1} for [Tm] = 4 mol %, using $\tau = 2.92$ ms and $\tau_d = 4.42$ ms.

Tellurite glasses have shown efficient emission at $\sim$2 μm from Tm^{3+}-doped and Tm^{3+}, Ho^{3+} -doped tellurite glass optical fiber lasers.[2,3,26,27] The results presented in this investigation indicate that perhaps the main issue impeding the efficiency of these fiber lasers is water incorporation and the low luminescence efficiency of the $^3F_4$ level in the more concentrated (i.e., > 2 mol %) Tm^{3+}-doped samples. To illustrate this, we have carried out a numerical simulation to predict the performance of Tm^{3+}-doped tellurite fiber lasers.

The profile of the second overtone (SO) absorption from free OH$^-$ radicals (the fundamental absorption feature is shown in Fig. 1(b)) was calculated and exhibited a wideband from 1300 to 1950 nm, which clearly overlaps with the $^3H_4 \rightarrow {}^3F_4$ and $^3F_4 \rightarrow {}^3H_6$ emission bands. The SO absorption from free OH$^-$ is difficult to measure because its absorption spreads across two fundamental absorption transitions, i.e., $^3H_6 \rightarrow {}^3H_5$ and $^3H_6 \rightarrow {}^3F_4$ of Tm^{3+} and it is relatively weak. Based on this argument, it is reasonable to assume that non-radiative energy transfer from the Tm^{3+}($^3H_4$) level to the SO of free OH$^-$ radicals occurs with a transfer rate having similar values to those relevant to Tm^{3+}($^3F_4$) $\rightarrow$ OH$^-$ transfer. The expected transfer rates, however, of 10 s^{-1} for [Tm^{3+}] = 2 mol % and 110 s^{-1} for [Tm^{3+}] = 4 mol % are small compared to the rates of CR observed to occur from the $^3H_4$ level, which are 5766 s^{-1} for [Tm^{3+}] = 1 mol %, 31 034 s^{-1} for [Tm^{3+}] = 2 mol % and 164 378 s^{-1} for [Tm^{3+}] = 4 mol % suggesting that Tm^{3+}($^3H_4$) $\rightarrow$ OH$^-$ transfer can be neglected, i.e., the luminescence quenching of the $^3H_4$ level is attributed to the CR process alone according to Eq. (5).

We will use a rate equation analysis to describe cw operation of Tm^{3+}-doped TZBG fiber lasers. Figure 7 shows the simplified energy level scheme used to describe the Tm^{3+}-doped TZBG laser system for cw laser pumping of the n_4 level (i.e., the $^3H_4$ manifold). n_1, n_2, n_3, and n_4 are the populations of the $^3H_6$, $^3F_4$, $^3H_5$, and $^3H_4$ manifolds of Tm^{3+}, respectively, and $n_1 + n_2 + n_3 + n_4 = 1$ and $n_{OH} = 1$. The population n_3 is considered negligible in tellurite glasses because we have not observed fluorescence near 1230 nm from the $^3H_5$ level under pulsed laser excitation at 794 nm or 1180 nm in Tm^{3+}-doped TZBG glass. This may be due to the strong multiphonon decay process, which quenches the expected fluorescence due to the small energy level separation of $\sim$2478 cm^{-1} to the next lower energy level, i.e., the $^3F_4$ level.

The rate equations were written to include the essential energy levels and pump and decay processes for laser
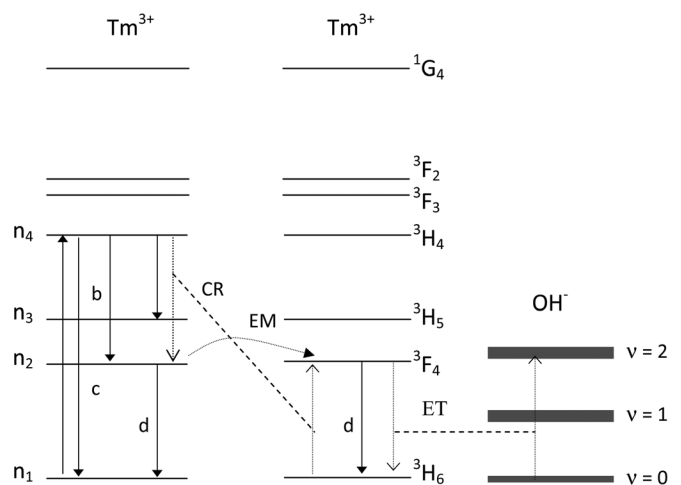

FIG. 7. A schematic of the energy levels diagram used for Tm^{3+}-doped TZBG glass under cw laser pumping at 794 nm (solid up-arrow). Radiative transitions are $a = 2335$ nm, $b = 1465$ nm ($\beta_{42} + \beta_{43}) = 0.103$, $c = 805$ nm ($\beta_{41} = 0.897$), and $d = 1865$ nm.

TABLE III. Experimental values of the intrinsic lifetime of $^3F_4$ (τ_d), radiative lifetime, radiative lifetime, luminescence branching ratios, cross-relaxation rate (W_{CR}), and $Tm^{3+} \rightarrow OH^-$ energy transfer (W_{OH}) used in the numeric simulation in TZBG glass.

Transition ($i \rightarrow j$)	$\bar{\lambda}$ (nm)	τ_R (ms)[a]	β_{ij}[a]
$^3H_4 \rightarrow {}^3H_6$ (4→1)	805	0.435	0.897
$^3H_4 \rightarrow {}^3F_4$ (4→2)	1465		0.076
$^3H_4 \rightarrow {}^3H_5$ (4→3)	2335		0.027
$^3F_4 \rightarrow {}^3H_6$ (2→1)	1865	2.71	1
[Tm^{3+}] (mol %)	τ_d (ms)[b]	W_{CR} (s^{-1})	W_{OH} (s^{-1})
0.5	4.01	1262	~0
1	4.32	5768	~0
2	4.41	31037	10
4	4.42	164370	116

[a]Radiative lifetime and branching ratios calculated using J-O theory.
[b]Intrinsic lifetime of the $^3F_4$ level obtained from using the critical radius model.

emission at 1865 nm or 2335 nm when the $^3H_4$ level is excited by pump radiation. The rate equations are

$$\frac{dn_1}{dt} = -R_P n_1 + \frac{n_2}{\tau_d} + \frac{B_{41}}{\tau_{R4}} n_4 - W_{CR} n_4 n_1 + W_{OH} n_2, \quad (8)$$

$$\frac{dn_2}{dt} = -\frac{n_2}{\tau_d} + \frac{(\beta_{42} + \beta_{43})}{\tau_{R4}} n_4 + 2W_{CR} n_4 n_1 - W_{OH} n_2, \quad (9)$$
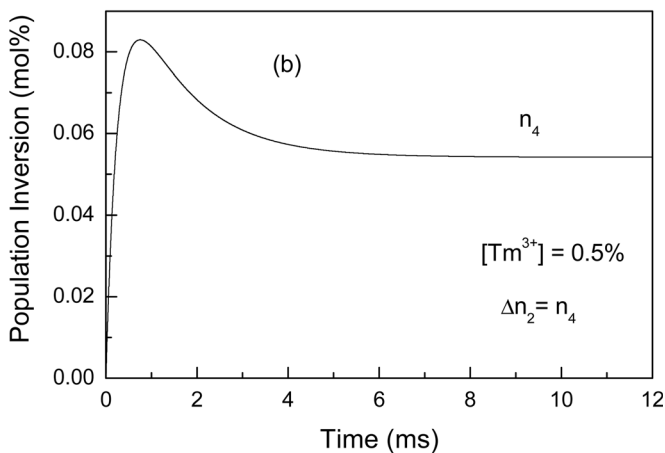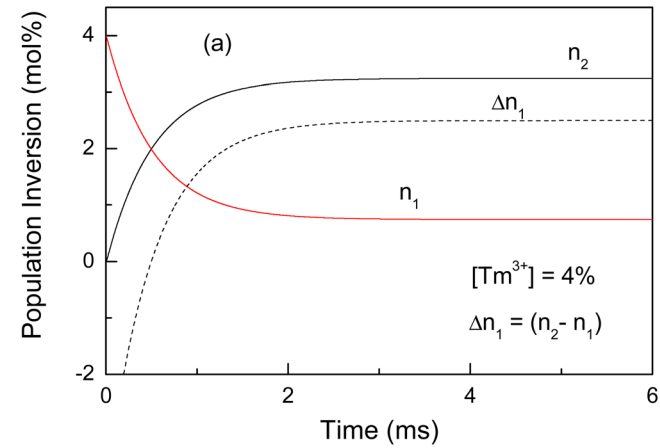

FIG. 8. Calculated evolution of the excited state populations (in mol %) of Tm^{3+} for (a) 1865 nm, [Tm^{3+}] = 4 mol % and (b) 2335 nm, [Tm^{3+}] = 0.5 mol % using a pumping rate $R_P = 800$ s^{-1} (or $I_P = 19.6$ kW cm^{-2}).

$$\frac{dn_4}{dt} = R_P n_1 - \frac{n_4}{\tau_{R4}} - W_{CR} n_4 n_1, \quad (10)$$

where $R_P = \sigma_{14} (I_P / h\nu_P)$ is the pump rate (s^{-1}), I_P is the intensity of the pump light (in W cm^{-2}), and $h\nu_P$ is the photon energy of the pump radiation and $\sigma_{14} = 1.02 \times 10^{-20}$ cm^2 at 794 nm. b_{ij} represents the luminescence branching ratio and τ_{Ri} is the radiative lifetime of the $^3F_4$ and $^3H_4$ excited states where $i = 2, 3, 4$, respectively. Experimental values of the intrinsic lifetime (τ_d) of the $^3F_4$ level and radiative lifetime (τ_{R4}) and the luminescence branching ratios ($\beta_{41}, \beta_{42}, \beta_{43}$), the cross-relaxation rate (W_{CR}) and W_{OH} as a function of [Tm^{3+}] in TZBG glass are listed in Table III.

The calculated evolution of the excited state populations (in mol %) obtained by numerical simulation of the rate equations for Tm^{3+}(0.5 and 4 mol %)-doped TZBG glass using a cw pumping rate of 800 s^{-1} (or $I_P = 19.6$ kW cm^{-2}) at 794 nm is shown in Fig. 8, where one can see that equilibrium is reached within $t \leq 4$ ms [see Fig. 8(a)] for laser emission at 1865 nm using [Tm^{3+}] = 4 mol % and within $t \leq 10$ ms [see Fig. 8(b)] for laser emission at 2335 nm having [Tm^{3+}] = 0.5 mol %. At equilibrium, the populations n_3, n_2,
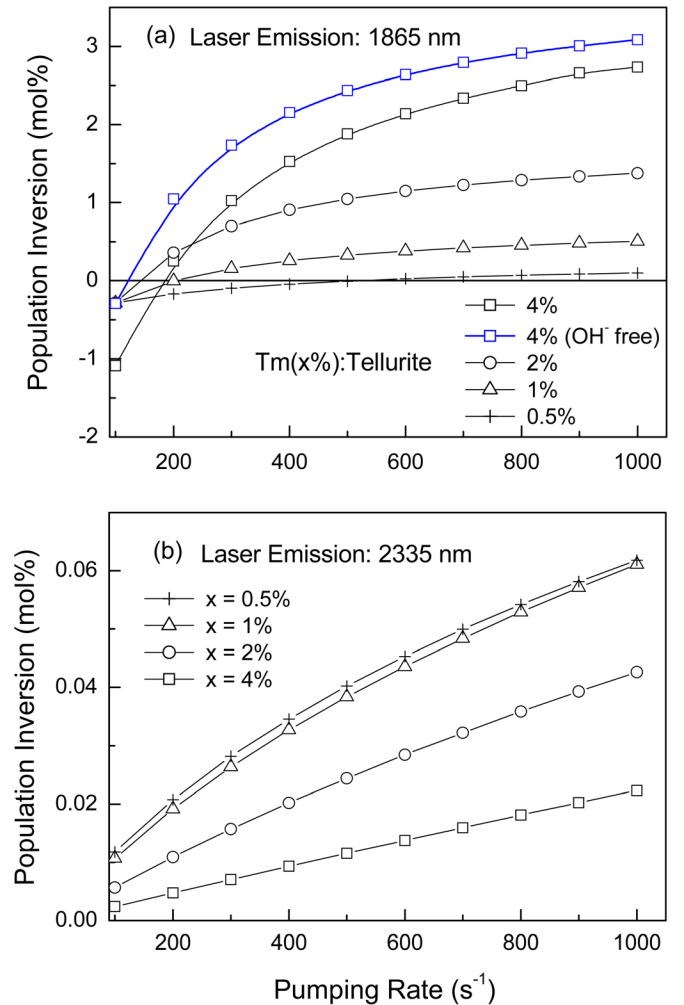

FIG. 9. Calculated population inversion (in mol %) for laser emission at (a) 1865 nm and (b) 2335 nm obtained for $Tm^{3+}(x)$-doped TZBG glass with $x = 0.5, 1, 2,$ and 4 mol %. One can find the equivalent pumping intensity (I_P) using the relation I_P(kWcm^{-2}) $= 0.02453 \times R_P$(s^{-1}).

and n_1 were taken and the population inversions $\Delta n_1 = n_2 - n_1$ and $\Delta n_2 = (n_4 - n_3) \sim n_4$ (because n_3 i.e., $^3H_5$ population is negligible) were obtained for $[Tm^{3+}] = 0.5, 1, 2,$ and 4 mol % as a function of the pump intensity at 794 nm; these results are presented in Figs. 9(a) and 9(b). Figure 9(a) shows that the laser emission at 1865 nm has a maximum population inversion Δn_1 for $[Tm^{3+}] = 4$ mol % exhibiting a threshold pump intensity of 4.5 kW cm^{-2} (or 184.6 s^{-1}). The threshold pumping intensity decreases to 3 kW cm^{-2} for laser emission at 1865 nm for the $[Tm^{3+}] = 4$ mol % sample if we set the $W_{OH} = 0$, i.e., for a hypothetically OH-free sample, as is shown by the blue colored curve in Fig. 9(a). On the other hand, laser emission at 2335 nm has maximum population inversion (i.e., Δn_2) for $[Tm^{3+}] = 0.5$ mol % and a negligibly small threshold pump intensity; see the results presented in Fig. 9(b).

To create a fiber laser based on the $^3H_4 \rightarrow {}^3H_5$ laser transition which has a low luminescence efficiency ($\eta_1 = 1.74\%$ for $[Tm^{3+}] = 0.5\%$) in Tm^{3+}-doped (tellurite or fluoride) glass one must fabricate a fiber glass that is 1 (or 2) meters long and pump using a diode laser emitting at 792 nm. This laser transition has the advantage of being a four level system with the lower laser level ($^3H_5$) rapidly de-exciting to the next lower level (F_4 level) thus avoiding bottlenecking that is detrimental for cw operation. A population inversion of 53% can be obtained for square pump pulses of 760 μs duration; see in Fig. 8(b) which shows the maximum population inversion for the $^3H_4 \rightarrow {}^3H_5$ transition occurs near $t \sim 758$ μs.

V. CONCLUSION

It has been determined that the luminescence efficiency of the $^3H_5 \rightarrow {}^6H_6$ transition at $\sim$1230 nm in Tm^{3+}-doped TZBG glass at T = 300 K is negligibly small which is primarily the result of large rates of multiphonon emission which forces the nonradiative decay rate to be much bigger compared to the calculated radiative rate decay of 499 s^{-1}. The decay time of the $^3H_4$ level is concentration dependent which we attribute to the well-known CR process, which is assisted by excitation migration. Emission from the $^3F_4$ level (at 1865 nm) displayed an increase in the decay time with $[Tm^{3+}]$ due to energy migration that also obeyed the critical radius model with a critical concentration calculated to be 0.35 mol %. The decay time of the $^3F_4$ level was observed to decrease in the highly concentrated sample as a result of energy transfer to OH$^-$ free radicals transfer with a rate determined to be $W_{OH} = 116$ s^{-1}. The presence of free OH$^-$ radicals was observed in the infrared absorption spectrum with an average OH$^-$ concentration of 1.6×10^{18} cm^{-3}. Despite the presence of OH$^-$, we calculated that all concentrations allow a population inversion for emission at 1865 nm

with the sample having $[Tm^{3+}] = 4$ mol % having the highest gain as a result of cross relaxation with a threshold pumping intensity (at 794 nm) of 4.5 kW cm^2. Likewise, we calculated that all concentrations allow a positive population inversion for emission at 2335 nm and that the highest gain was obtained for $[Tm^{3+}] = 0.5$ mol %.

[1]S. D. Jackson and T. A. King, Opt. Lett. **23**, 1462 (1998).
[2]B. Richards, A. Jha, Y. Tsang, D. Binks, J. Lousteau, F. Fusari, A. Lagatsky, C. Brown, and W. Sibbett, Laser Phys. Lett. **7**, 177 (2010).
[3]K. F. Li, G. A. Zhang, and L. L. Hu, Opt. Lett. **35**, 4136 (2010).
[4]N. K. Giri, A. K. Singh, and S. B. Rai, J. Appl. Phys. **101**, 033102 (2007).
[5]L. D. da Vila, L. Gomes, C. R. Eyzaguirre, E. Rodriguez, C. L. Cesar, and L. C. Barbosa, Opt. Mater. **27**, 1333 (2005).
[6]R. Balda, J. Fernández, and J. M. Fernández-Navarro, Opt. Express **17**, 8781 (2009).
[7]Bo Zhou, Hai Lin, and Edwin Yue-Bun Pun, Opt. Express **18**, 18805 (2010).
[8]M. Naftaly, S. Shen, and A. Jha, Appl. Opt. **39**, 4979 (2000).
[9]J. Wu, Z. Yao, J. Zong, and Sh. Jiang, Opt. Lett. **32**, 638 (2007).
[10]N. Spector and R. Reisfeld, Chem Phys. Lett. **49**, 49 (1977).
[11]J. S. Wang, E. Snitzer, E. M. Vogel, and G. H. Sigel, J. Lumin. **60–1**, 145 (1994).
[12]L. H. Huang, S. X. Shen, and A. Jha, J. Non. Cryst. Solids **345**, 349 (2004).
[13]S. D. Jackson, Opt. Commun. **230**, 197 (2004).
[14]M. Arnaudov, Y. Dimitriev, V. Dimitrov, and M. Dimitrovapankoval, Phys. Chem. Glasses **27**, 48 (1986).
[15]L. Nemec and J. Gotz, J. Am Ceram. Soc. **53**, 526 (1970).
[16]X. Feng, S. Tanabe, and T. Hanada, J. Non-Cryst. Solids **281**, 48 (2001).
[17]R. Rolli, M. Montagna, S. Chaussedent, A. Monteil, K. V. Tikhomirov, and M. Ferrari, Opt. Mater. **21**, 743 (2003).
[18]B. M. Walsh, N. P. Barnes, D. J. Reichle, and S. Jiang, J. Non-Cryst. Solids **352**, 5344 (2006).
[19]E. R. Taylor, L. N. Ng, N. P. Sessions, and H. Buerger, J. Appl. Phys. **92**, 112 (2002).
[20]Y. G. Choi, D. H. Cho, and K. H. Kim, J. Non-Cryst. Solids **276**, 1 (2000).
[21]C. A. Evans, Z. Ikonic, B. Richards, P. Harrison, and A. Jha, J. Lightwave Technol. **27**, 4280 (2009).
[22]V. K. Takhomirov, J. Mendez-Ramos, V. D. Rodriguez, D. Furniss, and A. B. Seddon, J. Alloys Compd. **436**, 216 (2007).
[23]A. I. Burshtein, JETP Lett. **35**, 885 (1972).
[24]A. Braud, S. Girard, D. L. Doualan, M. Thuau, R. Moncorge, and A. M. Tkachuk, Phys. Rev. B **61**, 5280 (2000).
[25]M. J. Weber, Phys. Rev. B **4**, 2932 (1971).
[26]J. S. Wang, E. Snitzer, E. M. Vogel, and G. H. Sigel Jr., J. Lumin. **60–61**, 145 (1994).
[27]Y. Tsang, B. Richards, D. Binks, J. Lousteau, and A. Jha, Opt. Lett. **33**, 1282 (2008).